Supporting materials

Catalyst-free oxidation of nitrogen fixation by underwater bubble discharge: performance optimization and mechanism exploration

Zi-Kai Zhou, Shu-Qi Li, Chao-Jun Chen, Yao Li, Xiao-Qiong Wen*, De-Zheng Yang*

Key Lab of Materials Modification by Laser, Ion, and Electron Beams Dalian University of Technology, Ministry of Education, Dalian, 116024, People' Republic of China

*Corresponding author. E-mail address:

wenxq@dlut.edu.cn (Xiao-Qiong Wen)

yangdz@dlut.edu.cn (De-Zheng Yang)

Bubble Characterization Methodology

Bubble size was determined by taking photographs of bubbles emerging from a coaxial discharge reactor in an optically transparent quartz vessel. The captured bubble images were processed using Fiji (Fiji Is Just ImageJ) image processing software by enhancing the contrast between the glowing bubbles and the background for size analysis using the Weka plug-in in the software.

The Weka Segmentation machine learning algorithms were trained to classify the illuminated bubbles and backgrounds as separate segments. Bubbles are then manually adjusted to eliminate any misidentified bubbles caused by multiple bubbles overlapping or visual artefacts in the photo.

The frequency of each bubble diameter from 0-5 mm in diameter was divided into 0.1 mm increments and the distribution was analyzed to characterize a total of 1500 bubbles between 15 images and The Sauter mean diameter (SMD) following equation S1 was used to represent the mean diameter of the characterized bubbles.

$$SMD = \frac{\sum_{i=1}^{N} n_i d_i^3}{\sum_{i=1}^{N} n_i d_i^2} \qquad \text{(S1)}$$

SMD= Sauter Mean Diameter (mm)

N= Total number of bubbles characterised

n_i= Number of bubbles in size range i

d_i= Diameter of bubble in size range i (mm)

At flow rates above 1 SLM occasional coalescence of adjacent micro-bubbles (Ø > 1.6 mm) was observed. The resulting enlargement and breakup of bubbles modulated the instantaneous gap length, leading to small (< 5 %) fluctuations in discharge current but no sustained instability. This behavior accounts for the slight reduction in NO_x^- yield at the highest flow rates (Fig. 4a) and confirms that bubble-size control is beneficial for maintaining a steady spark channel.

The reduced electric field in the bubble discharge

To ensure stable functionality in ZDPlaskin simulations, it is necessary to adopt an approximation wherein the reduced electric field and electron density are assumed to be constant. This simplification can result in an overestimation of ion densities, sometimes exceeding the electron density. Nevertheless, if ion-related reactions do not significantly influence the overall reaction mechanism, this approximation has a negligible impact on the accuracy of the simulation outcomes. We solve for this using the following equation(S2)

$$\frac{E}{N} = \frac{1}{N} \bullet \sqrt{\frac{P(t)}{\sigma}} \quad \text{(S2)}$$

Electron conductivity (σ) can be calculated as a function of electron density and electron mobility, the latter of which can be obtained from BOLSIG+.

Zero-D plasma chemistry modelling

The model takes into account parameters of the reactor structure such as the diameter of the high-voltage electrodes, and the solution volume to self-consistently calculate the reduced electric field based on the voltage-current waveforms measured in various discharge modes (Fig. S2) and is used as an input parameter to reveal the transient plasma properties with a reasonable computational load.

Table S1. Summarized important gas phase reactions in N_2/O_2 plasma system; the gas temperature T_{gas}

	Process	Rate coefficient [cm^3s^{-1}] [cm^6s^{-1}] ǂ	Ref.
Deactivation of O metastable			
R1	$O(1D) + O_2 => O + O_2$	6.4d-12 * exp(67.0d0/T_{gas})	[1]
R2	$O(1D) + O_2 => O + O_2(a1)$	1.0d-12	[1]
R3	$O(1D) + O_2 => O + O_2(b1)$	2.6d^{-11} * exp(67.0d0/T_{gas})	[1]
R4	$O(1D) + N_2 => O + N_2$	2.3d-11	[1]
R5	$O(1D) + O_3 => O_2 + O + O$	1.2d-10	[1]
R6	$O(1D) + O_3 => O_2 + O_2$	1.2d-10	[1]
R7	$O(1D) + NO => O_2 + N$	1.7d-10	[1]
R8	$O(1D) + N_2O => NO + NO$	7.2d-11	[1]
R9	$O(1D) + N_2O => O_2 + N_2$	4.4d-11	[1]
R10	$O(1S) + O => O + O$	5.0d-11 * exp(-73.0d0/T_{gas})	[1]
R11	$O(1S) + N => O + N$	1.0d-12	[2]
R12	$O(1S) + N => O + N$	1.0d-12	[1]
R13	$O(1S) + O_2 => O(1D) + O_2$	1.24d-12 * exp(-208.0d0/T_{gas})	[1]
R14	$O(1S) + O_2 => O + O + O$	3.0d-12 * exp(-850.0d0/T_{gas})	[1]
R15	$O(1S) + O_2 => O + O_2(4.5eV)$	2.76d-12 * exp(-208.0d0/T_{gas})	[1]
R16	$O(1S) + N_2 => O + N_2$	5.0d-17	[1]
R17	$O(1S) + NO => O + NO$	2.9d-10	[1]
R18	$O(1S) + NO => O(1D) + NO$	5.1d-10	[1]
R19	$O(1S) + O_3 => O_2 + O_2$	2.9d-10	[1]
R20	$O(1S) + N_2O => O + N_2O$	6.3d-12	[1]
R21	$O(1D) + O => O + O$	8.0d-12	[1]
R22	$O(1S) + O => O + O$	7.5d-12	[3,4]
Bimolecular nitrogen-oxygen reactions			
R23	$N + NO => O + N_2$	1.8d-11 * (T_{gas}/300.0)*0.5	[1]
R24	$N + O_2 => O + NO$	3.2d-12 * (T_{gas}/300.0) * exp(-3150.0d0/T_{gas})	[1]
R25	$N + NO_2 => O + O + N_2$	9.1d-13	[1]
R26	$N + NO_2 => O + N_2O$	3.0d-12	[1]
R27	$N + NO_2 => N_2 + O_2$	7.0d-13	[5]
R28	$N + NO_2 => NO + NO$	2.3d-12	[1]
R28	$O + N_2 => N + NO$	3.0d-10 * exp(-38370.0d0/T_{gas})	[1]
R29	$O + NO => N + O_2$	7.5d-12 * (T_{gas}/300.0) * exp(-19500.0d0/T_{gas})	[1]
R30	$O + NO => NO_2$	4.2d-18	[1]
R31	$O + N_2O => N_2 + O_2$	8.3d-12 * exp(-14000.0d0/T_{gas})	[1]
R32	$N_2 + O_2 => O + N_2O$	2.5d-10 * exp(-50390.0d0/T_{gas})	
R33	$NO + NO => O + N_2O$	2.2d-12 * exp(-32100.0d0/T_{gas})	
R34	$NO + O_2 => O + NO_2$	2.8d-12 * exp(-23400.0d0/T_{gas})	
R35	$NO + N_2O => N_2 + NO_2$	4.6d-10 * exp(-25170.0d0/T_{gas})	
R36	$NO_2 + NO_2 => NO + NO + O_2$	3.3d-12 * exp(-13500.0d0/T_{gas})	
R37	$NO_3 + O_2 => NO_2 + O_3$	1.5d-12 * exp(-15020.0d0/T_{gas})	
R38	$NO_3 + NO_3 => O_2 + NO_2 + NO_2$	4.3d-12 * exp(-3850.0d0/T_{gas})	
Dissociation of nitrogen-oxygen molecules			
R39	N_2 + @M => N + N + @M @M = N_2 O_2 NO O N @R = 1.0d0 6.6d0	5.4d-8 * (1.0d0-exp(-3354.0d0/T_{gas})) * exp(-113200.0d0/T_{gas}) * @R	
R40	O_2 + @M => O + O + @M @M = N_2 O_2 O N NO @R = 1.0d0 5.9d0 21.d0 1.0d0	6.1d-9 * (1.0d0-exp(-2240.0d0/T_{gas})) * exp(-59380.0d0/T_{gas}) * @R	[1]
R41	NO + @M => N + O + @M @M = N_2 O_2 O N NO @R = 1.0d0 20.0d0	8.7d-9 * exp(-75994.0d0/T_{gas}) * @R	[1]
R42	O_3 + @M => O_2 + O + @M @M = N_2 O_2 N @R = 1.0d0 0.38d0	6.6d-10 * exp(-11600.0d0/T_{gas}) * @R	[1]

R43	N_2O + @M => N_2 + O + @M @M = N_2 O_2 NO N_2O @R = 1.0d0 2.0d0 4.0d0	1.2d-8 * (300.0d0/T_{gas}) * exp(-29000.0d0/T_{gas}) * @R	[1]
R44	NO_2 + @M => NO + O + @M @M = N_2 O_2 NO NO_2 @R = 1.0d0 0.78d0 7.8d0 5.9d0	6.8d-6 * (300.0d0/T_{gas}) *2 * exp(-36180.0d0/T_{gas}) * @R	[1]
R45	NO_3 + @M => NO_2 + O + @M @M = N_2 O_2 NO N O @R = 1.0d0 10.0d0	3.1d-5 * (300.0d0/T_{gas}) *2 * exp(-25000.0d0/T_{gas}) * @R	[1]
R46	NO_3 + @M => NO + O_2 + @M @M = N_2 O_2 NO N O @R = 1.0d0 12.0d0	6.2d-5 * (300.0d0/T_{gas}) *2 * exp(-25000.0d0/T_{gas}) * @R	[1]
<u>Negative ion reactions</u>			
R47	O^- + O_2(a1) => O_2^- + O	1.0d-10	[1]
R48	O^- + O_3 => O_3^- + O	8.0d-10	[1]
R49	O^- + NO_2 => NO_2^- + O	1.2d-9	[1]
R50	O^- + N_2O => NO^- + NO	2.0d-10	[1]
R51	O^- + N_2O => N_2O^- + O	2.0d-12	[1]
R52	O_2^- + O => O^- + O_2	3.3d-10	[1]
R53	O_2^- + O_3 => O_3^- + O_2	3.5d-10	[1]
R54	O_2^- + NO_2 => NO_2^- + O_2	7.0d-10	[1]
R55	O_2^- + NO_3 => NO_3^- + O_2	5.0d-10	[1]
R56	O_3^- + O => O_2^- + O_2	1.0d-11	[1]
R57	O_3^- + NO => NO_3^- + O	1.0d-11	[1]
R58	O_3^- + NO => NO_2^- + O_2	2.6d-12	[1]
R59	NO^- + N_2O => NO_2^- + N_2	2.8d-14	[1]
R60	NO_2^- + NO_3 => NO_3^- + NO_2	5.0d-10	[1]

All 3-body reactions are in the unit of [cm^6 s^{-1}], 2.d0=2e0

Table S2. Summarized important liquid phase reactions in $N_2/O_2/H_2O$ plasma system

	Process	Rate coefficient [cm^3s^{-1}] [cm^6s^{-1}]ǂ	Ref.
<u>Ions</u>			
R1	e(aq) + H_2O(aq) => H_2O(aq)^-	5.e-15	[1]
R2	N_2(aq)^+ +H_2O(aq)=> H_2O(aq)^+ + N_2(aq)	1.0e-12	[1]
R3	N(aq)^+ + H_2O(aq) => H_2O(aq)^+ + N(aq)	5.e-15	[1]
R4	O_2(aq)^+ + H_2O(aq) => H_2O(aq)^+ + O_2(aq)	5.e-15	[1]
R5	NO(aq)^+ + H_2O(aq) => H_2O(aq)^+ + NO(aq)	5.e-15	[1]
R6	H_2(aq)^+ + H_2O(aq) => H_2O(aq)^+ + H_2(aq)	5.e-15	[1]
R7	NO_2(aq)^+ + H_2O(aq) => H_2O(aq)^+ + NO_2(aq)	5.e-15	[1]
R8	N_4(aq)^+ +H_2O(aq) => H_2O(aq)^+ + N_2(aq) + N_2(aq)	5.e-15	[1]
R9	H(aq)^+ + H_2O(aq) => H_3O(aq)^+	5.e-15	[1]
R10	H(aq)^- + H_2O(aq) => H_2O(aq)^- + H(aq)	5.e-15	[2]
R11	O(aq)^- + H_2O(aq) => OH(aq)^- + OH(aq)	3.e-15	[1]
<u>Acid dissociation</u>			
R12	ONOOH(aq) + H_2O(aq) => H_3O(aq)^+ + ONOO(aq)^-	5.e-15	[1]
R13	ONOO(aq)^- + H_3O(aq)^+ => H_2O(aq) + ONOOH(aq)	1.75e-6	[1]
R14	HO_2(aq) + H_2O(aq) => H_3O(aq)^+ + O_2(aq)^-	1.43e-17	[1]
R15	H_3O(aq)^+ + O_2(aq)^- => HO_2(aq) + H_2O(aq)	5.e-11	[1]
R16	HNO_2(aq) + H_2O(aq) => H_3O(aq)^+ + NO_2(aq)^-	5.e-15	[5]
R17	H_3O(aq)^+ + NO_2(aq)^- => HNO_2(aq) + H_2O(aq)	6.81e-10	[1]
R18	HNO_3(aq)+ H_2O(aq) => H_3O(aq)^+ + NO_3(aq)^-	3.e-8	[1]
R19	H_3O(aq)^+ + NO_3(aq)^- => HNO_3(aq)+H_2O(aq)	7.e-16	[1]
R20	HO_2NO_2(aq) + H_2O(aq) => O_2NO_2(aq)^- + H_3O(aq)^+	5.e-15	[1]
R21	O_2NO_2(aq)^- + H_3O(aq)^+ => HO_2NO_2(aq) + H_2O(aq)	1.05e-7	
<u>Reactive oxygen species</u>			
R22	OH(aq) + H(aq) => H_2O(aq)	3.e-11	[1]

R23	$H_2O(aq)$^- + O(aq) => O(aq)^- + $H_2O(aq)$	3.e-11	[1]
R24	$H_2O(aq)$^- + $O_2(aq)$ => $O_2(aq)$^- + $H_2O(aq)$	3.e-11	[1]
R25	$H_2O(aq)$^- + OH(aq) => OH(aq)^- + $H_2O(aq)$	5.e-11	[1]
R26	$H_2O(aq)$^- + $H_2O_2(aq)$ => OH(aq) + OH(aq)^- + $H_2O(aq)$	2.e-11	[5]
R27	$H_2O(aq)$^- + O(aq)^- => OH(aq)^- + OH(aq)^-	2.e-11	[1]
R28	$H_2O(aq)$^- + $H_2O(aq)$^- => $H_2(aq)$ +OH(aq)^- +OH(aq)^-	1.e-11	[1]
R29	$H_3O(aq)$^+ + OH(aq)^- => H(aq) + OH(aq) + $H_2O(aq)$	1.e-10	[1]
R30	$H_2O(aq)$ => $H_2O(aq)$^+ + e(aq)	1.e-20	
R31	$H_2O(aq)$ => OH(aq) + H(aq)	1.e-20	
R32	OH(aq) + OH(aq) => $H_2O_2(aq)$	1.7e-11	
R33	OH(aq) + $H_2(aq)$ => H(aq) + $H_2O(aq)$	6.e-14	
R34	OH(aq) + $HO_2(aq)$ => $O_2(aq)$ + $H_2O(aq)$	2.e-11	
R35	OH(aq) + $H_2O_2(aq)$ => $HO_2(aq)$ + $H_2O(aq)$	1.e-13	
R36	OH(aq) + OH(aq)^- => O(aq)^- + $H_2O(aq)$	8.e-12	
R37	OH(aq) + O(aq)^- => $HO_2(aq)$^-	4.e-11	
R38	OH(aq) + $O_2(aq)$^- => $O_2(aq)$ + OH(aq)^-	1.5e-11	
R39	OH(aq) + $HO_2(aq)$^- => $HO_2(aq)$ + OH(aq)^-	1.5e-11	
R40	H(aq) + $H_2O(aq)$ => $H_2(aq)$ + OH(aq)	1.5e-21	
R41	H(aq) + H(aq) => $H_2(aq)$	1.5e-11	
R42	H(aq) + $HO_2(aq)$ => $H_2O_2(aq)$	3.e-11	
R43	H(aq) + $H_2O_2(aq)$ => OH(aq) + $H_2O(aq)$	1.5e-13	
R44	$O_3(aq)$ => $O_2(aq)$ + O(aq)	3.e-6	
R45	$O_3(aq)$ + OH(aq)^- => $O_2(aq)$^- + $HO_2(aq)$	1.16e-19	
R46	$O_3(aq)$ + $O_2(aq)$^- => $O_3(aq)$^- + $O_2(aq)$	2.66e-12	
Reactive nitrogen species			
R47	N(aq) + N(aq) => $N_2(aq)$	5.e-14	[1]
R48	N(aq) + $H_2O(aq)$ => NH(aq) + OH(aq)	6.93e-39	[1]
R49	NH(aq) + NO(aq) => $N_2O(aq)$ + H(aq)	1.3e-12	[1]
R50	O(aq)^+ + $N_2(aq)$ => NO(aq)^+ + N(aq)	1.2e-12	[1]
R51	NO(aq) + NO(aq) + $O_2(aq)$ => $NO_2(aq)$ + $NO_2(aq)$	6.28e-36	[1]
R52	NO(aq) + $NO_2(aq)$ + $H_2O(aq)$ => $HNO_2(aq)$ + $HNO_2(aq)$	5.55e-34	[1]
R53	$NO_3(aq)$ + $H_2O(aq)$ => $HNO_3(aq)$ + OH(aq)	4.8e-14	[1]
R54	NO(aq) + $HO_2(aq)$ => $HNO_3(aq)$	5.33e-12	[1]
R55	OH(aq) + $HNO_3(aq)$ => $NO_3(aq)$ + $H_2O(aq)$	2.17e-13	[1]
R56	$N_2O_4(aq)$ + $H_2O(aq)$ => $HNO_2(aq)$ + $HNO_3(aq)$	1.33e-18	[1]
R57	$N_2O_5(aq)$ + $H_2O(aq)$ => $NO_2(aq)$ + $NO_3(aq)$ + $H_2O(aq)$	1.4e-19	[1]
R58	$N_2O_5(aq)$ + $H_2O(aq)$ => $HNO_3(aq)$ + $HNO_3(aq)$	2.e-21	[1]
R59	$NO_2(aq)$^- + $N_2O(aq)$ => $NO_3(aq)$^- + $N_2(aq)$	5.e-13	
R60	$HO_2NO_2(aq)$ + $HNO_2(aq)$ => $HNO_3(aq)$ + $HNO_3(aq)$	1.99e-20	
R61	$HO_2NO_2(aq)$ => $HNO_2(aq)$ + $O_2(aq)$	7.e-4	
R62	$HO_2NO_2(aq)$ => $HO_2(aq)$ + $NO_2(aq)$	4.6e-3	
R63	$N_2O_5(aq)$ + $H_2O(aq)$ => ONOOH(aq) + ONOOH(aq)	2.e-21	[1]
R64	ONOOH(aq) + $H_2O(aq)$ => $H_3O(aq)$^+ + $NO_3(aq)$^-	2.9e-23	[1]

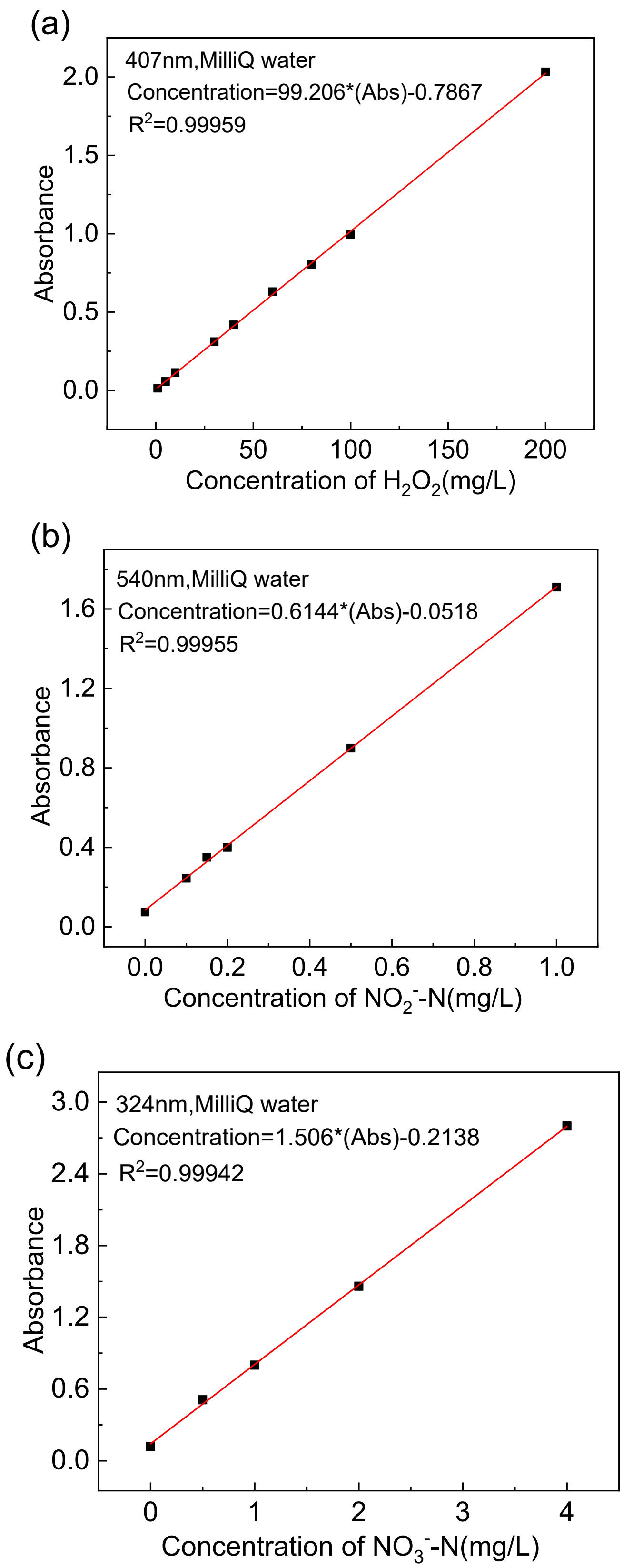

Fig. S1. (a) Standard curve for H_2O_2 detection using titanium salt photometry; (b) Standard curve for NO_2^- detection using ethylenediamine photometry; (c) Standard curve for NO_3^- detection using 2,6-dimethylphenol photometry

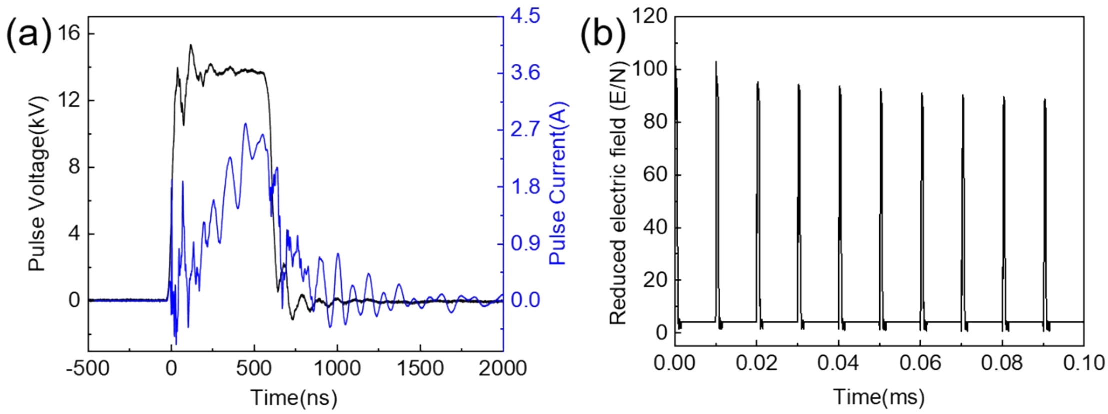

Fig. S2. (a) Voltage-current waveform of underwater bubble discharge; (b) Self-consistently derived corresponding the reduced electric field

In order to have a clearer understanding of the electric field distribution in the bubble discharge, the COMSOL transient electric field module was used without considering the plasma formation in order to analyze in depth the temporal and spatial evolution of the electric field, as shown in Fig. S3. In our reactor model, the tip edge of the high-voltage electrode is horizontally aligned with the air holes, which is also the same as the actual experimental configuration. With the addition of the applied voltage, affected by the pressure difference between the inside and outside, a potential difference of $1*10^6$ V/m is first formed inside the air holes, which is followed by a rapid spreading to the edge of the high-voltage electrode, and then gradually develops inside the bubbles, resulting in the formation of spark bubble discharge.

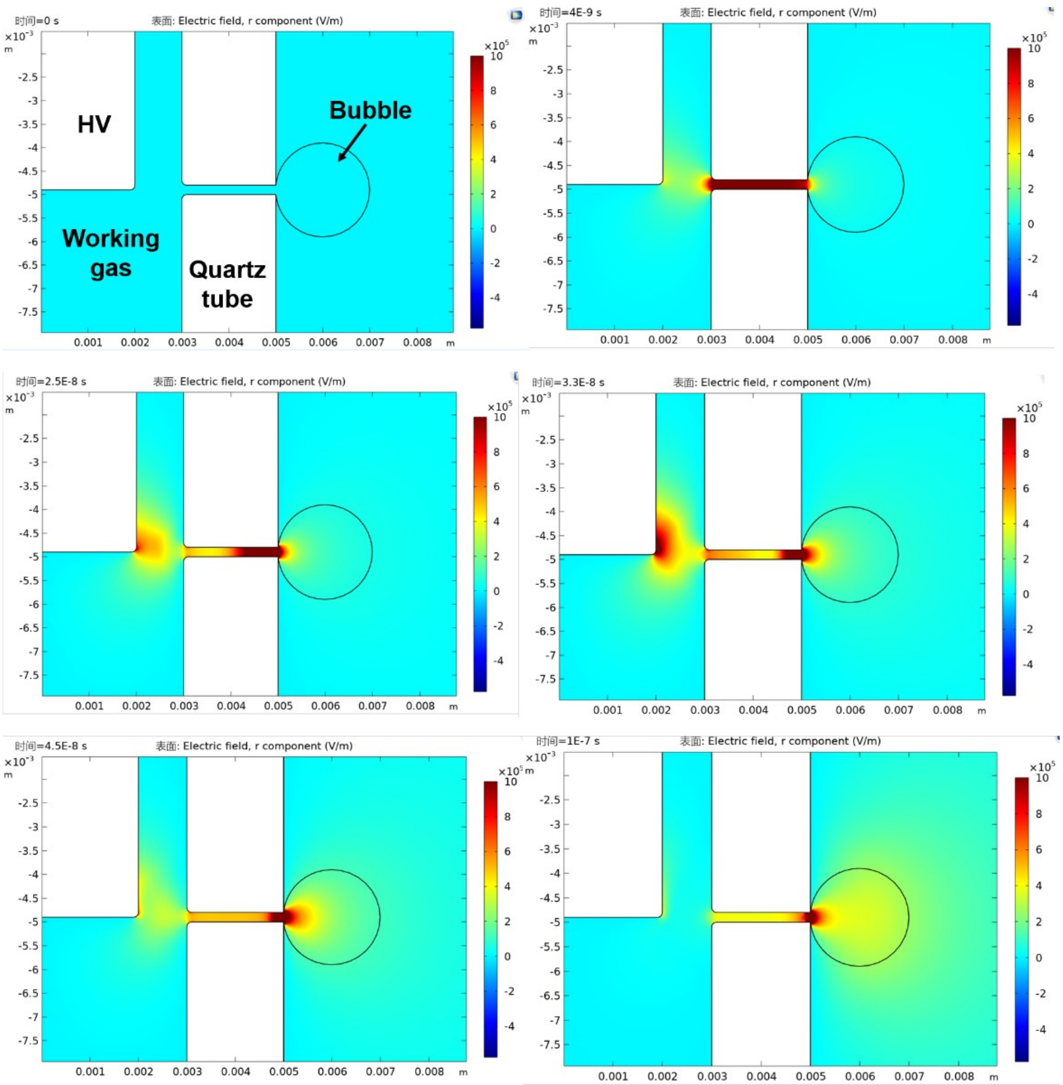

Fig. S3. Simulated electric field distribution in the bubble column reactor configuration.

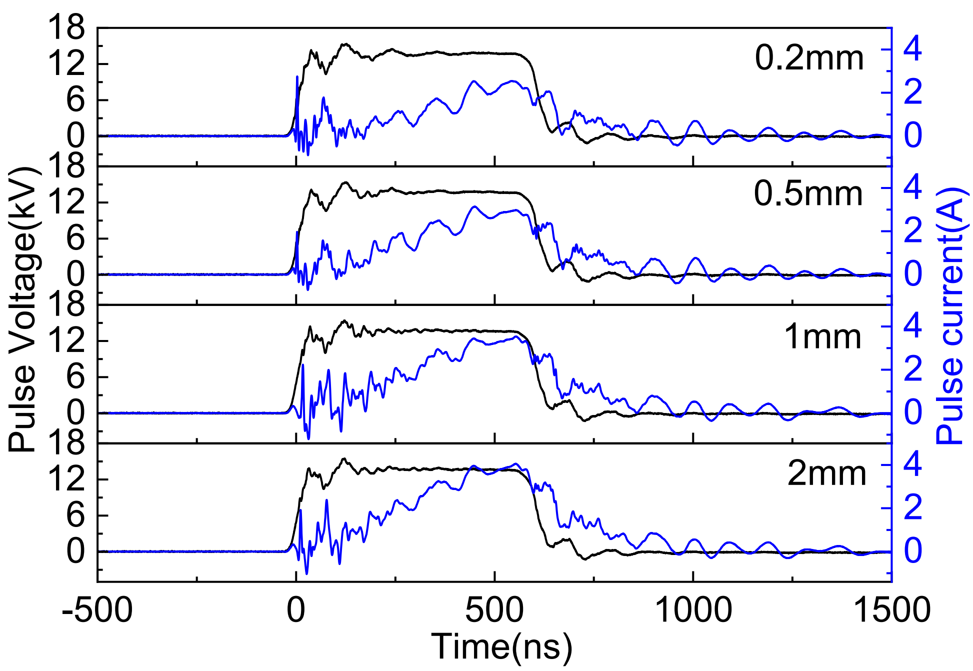

Fig. S4. Comparison of voltage and current waveforms with different pore diameters.

In order to clearly demonstrate the morphology of the bubbles at different air flow rates, we photographed the outgassing when they were not under discharge, and the bubbles show irregular channels at larger flow rates, which corresponds to lower gas-liquid mass transfer efficiencies, and that the bubbles at smaller flow rates can demonstrate a complete morphology while possessing lower diameters.

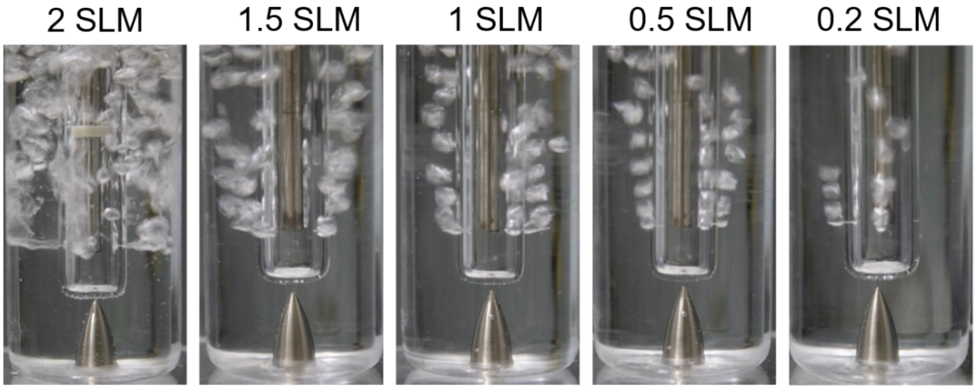

Fig. S5. Variation of bubble diffusion at different air flow rates (exposure time 1/125s)

REFERENCES

[1] Capitelli, M, Ferreira, C, Gordiets, B, and Osipov, A 2001 BOOK REVIEW: Plasma Kinetics in Atmospheric Gases *Plasma Physics and Controlled Fusion* 43 (3)371-372.

[2] Kossyi, I, Kostinskiy, A, Matveyev, A, and Silakov, V 1992 Kinetic scheme of the non-equilibrium discharge in nitrogen-oxygen mixtures *Plasma Sources Sci. Technol.* 1207-220.

[3] Itikawa, Y, and Mason, N 2005 Cross Sections for Electron Collisions with Water Molecules *J. Phys. Chem. Ref. Data* 341.

[4] Stafford, D S, and Kushner, M J 2004 $O_2(\Delta 1)$ production in He/O_2 mixtures in flowing low pressure plasmas *Journal of Applied Physics* 96 (5)2451-2465.

[5] Gordiets, B F, Ferreira, C M, Guerra, V L, Loureiro, J M A H, Nahorny, J, Pagnon, D, Touzeau, M, and Vialle, M 1995 Kinetic model of a low-pressure N_2/O_2 flowing glow discharge *IEEE Transactions on Plasma Science* 23 (4)750-768.